

# Seeking Physics in Diffusion Noise

Chujun Tang<sup>1</sup> Lei Zhong<sup>2</sup> Fangqiang Ding<sup>3\*</sup>

<https://thegreatestcj.github.io/Physics-in-Noise/>

<sup>1</sup>Brown University <sup>2</sup>University of Edinburgh <sup>3</sup>MIT

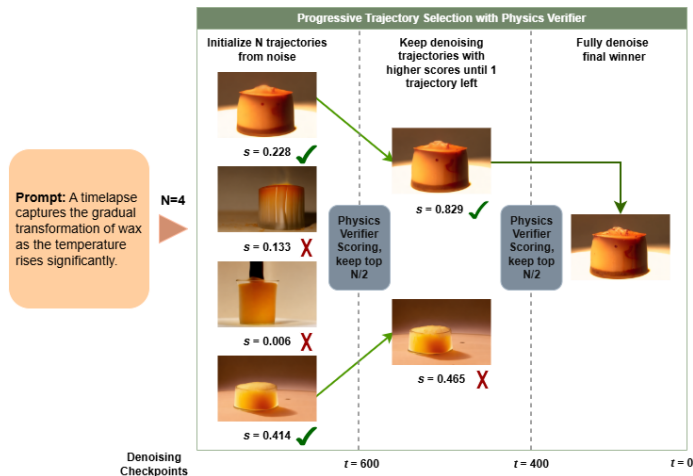


Fig. 1: **Progressive trajectory selection with a physics verifier.** Given a text prompt, we sample  $N$  denoising trajectories from different seeds and score each partially denoised sample at intermediate timesteps (e.g.,  $t=600, 400$ ) using a lightweight physics verifier applied to frozen DiT features. At each checkpoint we keep the top fraction (e.g.,  $N/2$ ) and terminate the rest early, continuing denoising only for the survivors until a single winner is fully denoised ( $t=0$ ).

**Abstract.** Do video diffusion models encode signals predictive of physical plausibility? We probe intermediate denoising representations of a pretrained Diffusion Transformer (DiT) and find that physically plausible and implausible videos are partially separable in mid-layer feature space across noise levels. This separability cannot be fully attributed to visual quality or generator identity, suggesting recoverable physics-related cues

\* Corresponding author. Email: [fding@mit.edu](mailto:fding@mit.edu)

in frozen DiT features. Leveraging this observation, we introduce progressive trajectory selection, an inference-time strategy that scores parallel denoising trajectories at a few intermediate checkpoints using a lightweight physics verifier trained on frozen features, and prunes low-scoring candidates early. Extensive experiments on PhyGenBench demonstrate that our method improves physical consistency while reducing inference cost, achieving comparable results to Best-of-K sampling with substantially fewer denoising steps.

## 1 Introduction

Video diffusion models [42,19,29,7] have recently achieved remarkable progress in generating visually realistic videos from text. Despite their strong visual fidelity and temporal coherence, recent systematic evaluations still reveal frequent violations of basic physical commonsense, including inconsistent gravity, collisions and object dynamics [18,26,3]. These findings highlight a persistent gap between perceptual realism and physical plausibility in current video generative models.

Existing solutions improve the physical consistency of generated videos either by adding external physical guidance beyond a frozen generator or by performing inference-time selection. External guidance typically comes from (i) *physics-conditioned generation*, which injects explicit physical priors as conditioning signals [23,41,45,14,24], or (ii) *physics-aware post-training*, which updates model weights via curated physics supervision/distillation [20,37,46,47] or preference/reward-based alignment [44,30,40,22]. While effective, these approaches require substantial training and often specialize to specific physical domains. Post-hoc selection offers an alternative at inference time: generate  $N$  candidate videos, score them with a vision-language model [2,27], and retain the best. Although Best-of- $N$  avoids retraining, it discards most sampled trajectories and incurs computational cost that scales linearly with  $N$ . Both paradigms implicitly assume that the generator does not already contain reliable cues about physical plausibility. In this work, we revisit this assumption and ask: *Does a frozen video diffusion model already encode signals predictive of physical plausibility in its intermediate representations?*

To investigate this question, we probe intermediate representations of a frozen video diffusion backbone (i.e., CogVideoX-2B [42]) along the denoising trajectory under varying noise levels, using human-labeled generated videos from diverse text-to-video generators [3]. We find that physically plausible and implausible videos become partially separable in mid-layer feature space, and, to our surprise, this separability per-

sists even at high noise levels. This observation suggests a simple but important implication: *if plausibility can be anticipated before denoising completes, we need not decode all the way to a final pixel-space video to decide which trajectories are worth continuing.* To assess this quantitatively, we train a lightweight verifier (1M parameters) on the frozen features. Despite its simplicity, it reliably distinguishes plausible from implausible videos (AUC  $\approx 0.68$ ), showing that intermediate representations already expose actionable cues for physical plausibility. Crucially, this cue cannot be reduced to superficial visual quality or generator bias: even when controlling for these confounders, the separation remains. This suggests that video diffusion models spontaneously structure their internal feature space in ways that reflect physical plausibility—an emergent signal we can exploit for more efficient, physics-aware generation.

Building on this implication, we propose *progressive trajectory selection*, a simple inference-time *selection* strategy that accelerates sampling for video generation while improving physical consistency. Instead of generating complete videos before scoring, we estimate plausibility *during* denoising and terminate weak candidates early (cf. Fig. 1). Concretely, we maintain  $N$  denoising trajectories in parallel and apply a lightweight physics verifier—trained on frozen DiT features at matched noise levels—at a small set of checkpoint timesteps. At each checkpoint, the verifier ranks the active trajectories using their intermediate frame-level representations, and we retain only the top candidates, pruning the rest for early termination (cf. Fig. 1). Since the verifier operates on intermediate features already produced by the backbone forward pass, it adds negligible overhead and, unlike gradient-based classifier guidance [12,43], requires no backpropagation through the generator.

Empirically, our progressive trajectory selection matches the overall physical consistency of standard Best-of- $K$  on PhyGenBench [23], while achieving stronger multi-frame physics and reducing inference cost via early termination of implausible trajectories. The method requires neither backbone retraining nor gradient-based guidance, making it lightweight and directly applicable to frozen video diffusion models. We summarize our contributions as follows:

- We perform a systematic probing study on frozen video diffusion model representations, demonstrating that physical plausibility is *linearly decodable* from intermediate denoising features, remains detectable *within* each source, and is most salient in mid-layer representations across moderate noise levels (Sec. 3).
- We introduce a compact, noise-aligned physical verifier and integrate it with progressive trajectory selection to score and early-stop low-

plausibility trajectories *during* denoising, improving the efficiency–quality trade-off without modifying or fine-tuning the backbone (Sec. 4).

- We conduct extensive experiments on PhyGenBench [23], where our method reduces inference time by 37% per prompt while maintaining performance comparable to Best-of- $K$ , analyze limitations and future directions, and will release code to support reproducibility and future research (Secs. 5, 6).

## 2 Related Work

### 2.1 Physics-Aware Video Generation

Prior work improves the physics awareness of video generators in two main ways: (i) conditioning generation on explicit physical priors, and (ii) updating the generator via post-training or fine-tuning. We review both lines of work below.

**Physics-conditioned generation.** One line of work introduces explicit physical priors as conditioning signals, including motion trajectories [23,41,13,48], forces/goals [14,15], structured dynamics or kinematic constraints [45,36,1,33], or material properties [24]. Such priors steer generation toward more physically grounded motion and interactions. For example, PhysGen [23] uses rigid-body simulation to generate trajectories that guide video synthesis, and NewtonGen [45] incorporates neural Newtonian dynamics as an explicit dynamics prior for physics-consistent, controllable motion. However, the achievable phenomena are ultimately bounded by the expressivity of the chosen priors; covering new regimes often requires new simulators/controllers or domain-specific supervision.

**Physics-aware post-training.** Another line of work strengthens the physics awareness of video generators by updating model parameters through additional training. One family performs supervised post-training on curated physics data or distillation signals to teach physical regularities [20,37,46,47]. For example, Pisa [20] fine-tunes video models on curated dropping-object videos to improve gravitational dynamics, while WISA [37] builds a physics-rule dataset for physics-aware generation. A second family performs preference/reward-based alignment using human or foundation-model feedback [44,30,8]. InstructVideo [44] applies RLHF based on human judgments of physical plausibility, and Prabhudesai et al. [30] propagate reward gradients from a learned scorer through the diffusion sampling process; related work further scales alignment with VLM/MLLM feedback or learned reward models [40,22,8]. Overall, while effective, post-training approaches typically

require substantial additional compute and produce model-specific weights, limiting direct applicability to *frozen* generators and transfer across architectures.

## 2.2 Inference-Time Scaling

Inference-time scaling improves generative quality without updating model weights by exploring multiple sampling trajectories at test time and selecting the most promising ones. In the video domain, DLBS [28] applies beam search with lookahead rollouts to obtain intermediate reward estimates, while EvoSearch [16] performs evolutionary search across diffusion- and flow-based generators. A central challenge is *intermediate scoring*: effective search requires a verifier whose early-time scores reliably predict final sample quality. In practice, however, reward models often correlate poorly with final quality during early denoising. Baraldi et al. [5] term this issue *verifier temporal coherence* and show that successive halving can underperform simple Best-of- $N$  when early scores are unreliable. This limitation is particularly acute for physical plausibility. Existing physics evaluators, such as PhyGenBench [26] and VideoScore [17], are most reliable on fully decoded videos and often require costly lookahead rollouts, limiting their usefulness as intermediate rewards for early trajectory pruning. In contrast, we ask whether physically relevant cues are already present in frozen diffusion representations, enabling plausibility estimation directly from intermediate noisy features and thereby supporting reliable early trajectory pruning.

## 3 Probing Physical Knowledge in Diffusion Noise

Post-hoc inference-time selection methods (e.g., Best-of- $N$ ) can improve physical plausibility by sampling multiple videos and choosing the best, but the benefit comes with a prohibitive cost: the compute scales linearly with  $N$  *full* denoising runs. Without a reliable intermediate signal, selection can only be performed *after* decoding complete videos, making physics-aware search expensive and limiting  $N$  in practice [5]. This motivates a key question: *does a frozen video diffusion model already encode physical knowledge in its intermediate denoising representations?* If such a signal is present early enough, we could score and prune trajectories *before* completion, *opportunistically* turning post-hoc selection into a more compute-efficient procedure. In this section, we investigate when and where physical knowledge emerges along the denoising process, laying the foundation for our accelerated trajectory selection in Sec. 4.

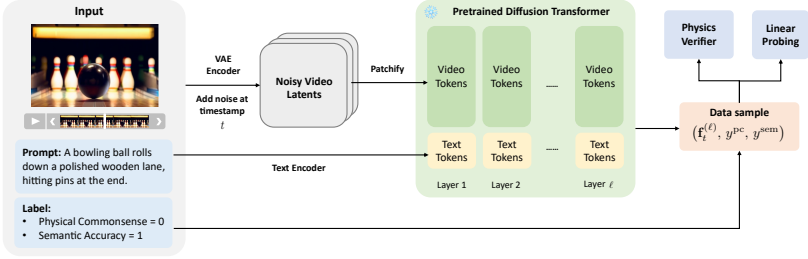


Fig. 2: **Feature extraction pipeline.** Given a generated video and its prompt, we encode the video with a VAE, add diffusion noise at timestep  $t$ , and run a frozen diffusion transformer. We extract hidden states at layer  $\ell$ , remove text-conditioning tokens, and spatially mean-pool video tokens to obtain per-frame features  $\mathbf{f}_t^{(\ell)} \in \mathbb{R}^{F \times D}$ . Each data sample is paired with PC and SA labels  $y^{PC}, y^{sem} \in \{0, 1\}$  and is used for linear probing (Sec. 3) and physics-verifier training (Sec. 4.1).

### 3.1 Setup

To probe whether intermediate denoising features encode physical commonsense, we extract features from a frozen video diffusion transformer (DiT), instantiated with CogVideoX-2B [42], on VideoPhy [3,4], a multi-source dataset of  $\sim 4,500$  videos generated by diverse text-to-video models, enabling a more general probe beyond any single generator. Each video is annotated by human raters with binary physical commonsense (PC) and semantic accuracy (SA) labels (cf. Fig. 2); unless otherwise specified, we focus on PC.

**Feature extraction.** Concretely, for each video, we first encode it into the VAE latent space [32], add diffusion noise at timesteps  $t \in \{200, 400, 600\}$  (larger  $t$  denotes noisier latents), and run a forward pass of the frozen DiT. For each timestamp, we extract hidden states after transformer block  $\ell \in \{5, 10, 15, 20, 25\}$ , remove text-conditioning tokens, and spatially mean-pool the remaining video tokens to obtain a per-frame feature sequence  $\mathbf{f}_t^{(\ell)} \in \mathbb{R}^{F \times D}$ , where  $F$  is the number of latent frames and  $D$  the hidden dimension. For linear probing, we flatten  $\mathbf{f}_t^{(\ell)}$  across time into a single feature vector. Figure 2 illustrates the pipeline used for both linear probing and subsequent physical verifier training.

**Linear probing protocol.** We quantify how much PC signal is present in the extracted representations via a simple linear probe. Specifically, we train a logistic regression linear classifier to predict the probability of the positive PC class from the feature vector of each video, and evaluate it using 5-fold cross-validation (5-fold CV). We report the mean AUC-

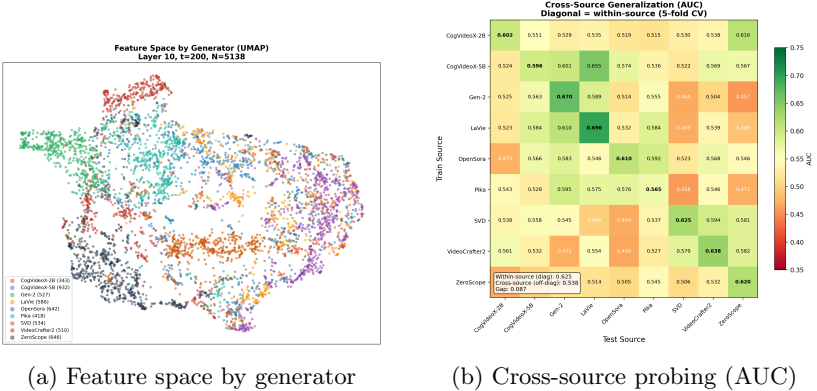


Fig. 3: **Source structure in DiT features.** (a) UMAP of CogVideoX-2B DiT features extracted after transformer block  $\ell=10$  at  $t=200$ , colored by the original video generator, reveals strong source clustering. (b) Cross-source probing AUC matrix (train  $\times$  test source): within-source evaluation (diagonal, 5-fold CV; mean 0.637) is substantially higher than cross-source transfer (off-diagonal mean 0.538).

ROC across folds. As a baseline, we run the *same* probing procedure on the raw noised VAE latents, without using any transformer features. This comparison isolates the contribution of the DiT: if DiT features outperform the latent-input baseline, it indicates that physics-related signal becomes more linearly accessible *through* denoising representations, beyond what is already present in the encoder latent space.

### 3.2 Disentangling Source and Physics Signals

Before attributing the linear probe performance in Sec. 3.1 to PC, we first inspect the geometry of the denoising feature space to identify potential confounders. A prominent factor is the *video source*, i.e., the original generator that produced the video. Since VideoPhy aggregates outputs from seven generators with distinct visual styles and artifacts, source-specific characteristics may induce strong structure in the learned representations. Figure 3a visualizes the CogVideoX-2B DiT features colored by generator identity. Videos cluster strongly by source, suggesting that generator-specific characteristics form a dominant structure in the representation space.

This raises a natural question: *does the PC signal detected by our probes merely reflect source identity?* To control for this factor, we train logistic regression probes *within* each source using 5-fold CV, i.e.,

Table 1: Within-source linear probing AUC (5-fold CV) using CogVideoX-2B [42] DiT features. We report results on the seven non-CogVideoX sources in VideoPhy [3].

	LaVie [39]	VideoCrafter2 [11]	ZeroScope [10]	Gen-2 [34]	OpenSora [49]	SVD [6]	Pika [20]	Overall
# Videos	528	468	612	477	610	492	376	3,563
AUC	0.712	0.631	0.613	0.612	0.597	0.579	0.534	0.652

Table 2: Linear probing AUC (5-fold CV) on DiT features extracted by the frozen CogVideoX-2B backbone. Gray subscripts show improvement over the VAE latent baseline at each timestep. Best per row in **bold**.

Timestep	VAE latent	$\ell=5$	$\ell=10$	$\ell=15$	$\ell=20$	$\ell=25$
$t=200$	0.539	0.569 (+.030)	<b>0.606</b> (+.067)	0.604 (+.065)	0.574 (+.035)	0.579 (+.040)
$t=400$	0.534	0.545 (+.011)	0.610 (+.076)	0.608 (+.074)	<b>0.624</b> (+.090)	0.594 (+.060)
$t=600$	0.537	0.565 (+.028)	<b>0.638</b> (+.101)	0.595 (+.058)	0.583 (+.046)	0.585 (+.048)

training and testing only on videos from the same generator. As shown in Table 1, PC-related separability remains detectable within every source (AUC 0.534–0.712), even after removing inter-source variation. This indicates that DiT features encode PC-relevant information beyond source identity, as a secondary signal beneath the dominant source structure.

At the same time, source identity remains a strong confounder for *transfer*. Figure 3b shows that probes trained on one generator generalize poorly to another (off-diagonal mean AUC 0.538), substantially below within-source performance (diagonal mean 0.637). We observe a similar degradation when transferring across backbones (CogVideoX-2B  $\rightarrow$  CogVideoX-5B), where AUC drops from  $\sim 0.62$  to  $\sim 0.55$ . These results motivate a *matched-distribution* strategy: our physical verifier is trained only on videos produced by the same generator/backbone used at inference time, so that it focuses on PC cues rather than generator-specific style statistics.

### 3.3 Layer and Timestep Analysis

Following the matched-distribution principle above, we restrict all subsequent analysis to videos generated by a single generator (i.e., CogVideoX-2B) and extract DiT features using its frozen backbone. Table 2 reports probing AUC across layers and noise levels. Several findings emerge.

**DiT features encode physics beyond VAE latents.** Across all configurations, DiT features outperform the VAE latent baseline, with

improvements of up to +0.101 at  $\ell=10$ ,  $t=600$ . This gap indicates that the DiT blocks amplify physics-relevant structure beyond what is recoverable from the raw VAE representation alone.

**Middle layers are most informative.** Among the probed layers,  $\ell=10$  achieves the highest AUC overall (0.638 at  $t=600$ ), while earlier ( $\ell=5$ ) and later ( $\ell=25$ ) layers carry weaker signal. This is consistent with findings in vision transformers, where middle layers often capture richer semantic structure before later layers become more specialized [31,9].

**Physics signal is robust across noise levels.** Contrary to the expectation that cleaner inputs ( $t=200$ ) would yield stronger separability, probing AUC remains comparable or even slightly higher at  $t=600$  for  $\ell=10$ . This suggests that physics-related structure remains recoverable at moderate noise levels, rather than being solely inherited from cleaner inputs.

### 3.4 Control Analyses

**DiT features vs. VAE latents.** A potential alternative explanation is that the PC signal originates *primarily* from the VAE encoder, rather than from the DiT. Beyond the CogVideoX-2B case study in Sec. 3.3, we applied the same control across all settings. We probe the raw noised VAE latents and find that DiT features consistently outperform them. The gap is particularly pronounced for LaVie-sourced videos (0.730 vs. 0.537), suggesting that physics-related structure becomes more linearly accessible through DiT representations than in the latent space alone. Please find more analysis in our supplementary materials.

**Disentangling from video quality.** Another concern is that physically plausible videos may also score better under generic automatic evaluators, causing the probe to rely on broad perceptual/alignment cues rather than physics. As a coarse control, we use VQAScore [21], a text-visual alignment metric assessing if the generated content matches the prompt. A logistic regression classifier trained solely on VQAScore achieves AUC 0.555, only slightly above chance. We remove the linearly VQAScore-correlated component of the features (via residualization) and repeat probing. The resulting AUC remains nearly unchanged, suggesting that the PC signal is not explained by this generic evaluator alone.

Taken together, these controls strengthen our interpretation that intermediate DiT features carry a genuine physics-related signal: it is enhanced by the DiT beyond the VAE latent input and is not explained by perceptual quality alone. This motivates the next question: *can such*

*intermediate signals be exploited during sampling to favor physically consistent outcomes?* In the next section, we show that a lightweight physical verifier trained on these features enables effective trajectory selection without modifying the backbone.

## 4 Method

The analyses in Section 3 indicate that frozen DiT features contain a recoverable signal correlated with physical plausibility. This signal is most prominent at intermediate layers, remains detectable under moderate noise, and is not explained by generic perceptual/alignment cues alone. At the same time, its transfer degrades across generators and backbones, motivating a matched-distribution strategy. We now describe how to exploit this signal at inference time.

**Overview.** Our method consists of two components. First, we train a lightweight *physics verifier* on frozen DiT features to estimate the physical plausibility of a trajectory based on intermediate representations extracted at selected denoising steps (cf. Section 4.1). Second, during inference, we maintain multiple sampling trajectories in parallel and progressively eliminate low-scoring candidates at predefined checkpoints, so that computation is concentrated on the most promising trajectories (cf. Section 4.2). Importantly, the verifier itself adds negligible per-trajectory overhead—it operates on features already computed in the standard forward pass and requires no backpropagation through the backbone.

**Notation.** We follow some symbol definition in Section 3.1. We denote the noisy latent at diffusion step  $t$  as  $\mathbf{z}_t$  and the text embedding as  $\mathbf{c}$ . We write  $\mathbf{h}_t^{(\ell)} \in \mathbb{R}^{S \times D}$  for the token-level hidden states after block  $\ell$ , and  $\mathbf{f}_t^{(\ell)} \in \mathbb{R}^{F \times D}$  for the resulting spatially pooled features used by our verifier.  $t \in \mathcal{T}$  and  $\ell \in \mathcal{L}$  denote candidate diffusion timesteps and transformer blocks, respectively, used for physics verifier training and progressive selection.

### 4.1 Physics Verifier

For each  $(t, \ell) \in \mathcal{T} \times \mathcal{L}$ , we first extract the corresponding frame-level feature sequence  $\mathbf{f}_t^{(\ell)}$  following the feature extraction pipeline described in Section 3.1.

**Causal temporal modeling.** Physical violations unfold over time and may affect subsequent frames. We therefore model temporal dependencies with a small causal self-attention module [38] over the per-frame sequence, using a triangular mask so that frame  $i$  attends only

to frames  $j \leq i$ . This prevents the verifier from exploiting future video frames when applied at intermediate denoising checkpoints. Concretely, we first project  $\mathbf{f}_t^{(\ell)} \in \mathbb{R}^{F \times D}$  to dimension  $d$  and add learnable positional embeddings:

$$\tilde{\mathbf{f}}_t^{(\ell)} = \text{Proj}(\mathbf{f}_t^{(\ell)}) + \mathbf{p}_{1:F} \in \mathbb{R}^{F \times d}, \quad (1)$$

where  $\text{Proj}(\cdot)$  is a linear layer. We then apply a single layer of causal multi-head self-attention with a residual connection:

$$\mathbf{y}_t^{(\ell)} = \tilde{\mathbf{f}}_t^{(\ell)} + \text{CausalAttn}(\text{LN}(\tilde{\mathbf{f}}_t^{(\ell)})), \quad (2)$$

where LN denotes LayerNorm and CausalAttn implements the triangular causal masking described above. As a result, the last-frame representation  $(\mathbf{y}_t^{(\ell)})_{F-1}$  provides a causally aggregated summary of the entire sequence.

**Classification.** We pass the last-frame representation  $(\mathbf{y}_t^{(\ell)})_{F-1}$  through a two-layer MLP preceded by LayerNorm to produce a physical plausibility score:

$$s_t^{(\ell)} = \text{Sigmoid}\left(\text{MLP}\left(\text{LN}\left((\mathbf{y}_t^{(\ell)})_{F-1}\right)\right)\right) \in [0, 1]. \quad (3)$$

Another head is trained with the same architecture to predict semantic accuracy.

**Training.** For each layer  $\ell \in \mathcal{L}$ , we train an individual verifier on VideoPhy [3], whose videos are annotated with binary labels for physical commonsense and semantic accuracy. For each video, we apply forward diffusion at timesteps  $t \in \mathcal{T}$  and extract the corresponding frame-level feature sequence  $\mathbf{f}_t^{(\ell)}$ . Let  $y^{\text{pc}}, y^{\text{sem}} \in \{0, 1\}$  denote the target labels, and let  $s_{t,\text{pc}}^{(\ell)}$  and  $s_{t,\text{sem}}^{(\ell)}$  be the outputs of the two heads. We optimize the verifier using the following training loss:

$$\mathcal{L}^{(\ell)} = \frac{1}{|\mathcal{T}|} \sum_{t \in \mathcal{T}} \mathbb{E} \left[ \lambda_{\text{pc}} \text{WBCE}(y^{\text{pc}}, s_{t,\text{pc}}^{(\ell)}) + \lambda_{\text{sem}} \text{WBCE}(y^{\text{sem}}, s_{t,\text{sem}}^{(\ell)}) \right] \quad (4)$$

where  $\text{WBCE}(y, s) = -w_y(y \log s + (1 - y) \log(1 - s))$  and  $w_y$  accounts for class imbalance.  $\lambda_{\text{pc}}$  and  $\lambda_{\text{sem}}$  balance the PC and semantic accuracy losses. Because the DiT backbone is frozen, feature extraction requires only a single forward pass per video per timestep. Further training details are provided in Section 5.1.

## 4.2 Progressive Trajectory Selection

Given the candidate layers  $\mathcal{L}$ , we select the best verifier layer  $\ell_{\text{best}}$  on the validation set and use the corresponding verifier for inference-time

---

**Algorithm 1** Progressive Trajectory Selection
 

---

**Require:** Text embedding  $\mathbf{c}$ ; number of trajectories  $N$ ; checkpoints  $\mathcal{C}$ ; keep ratio  $\rho$ ; selected layer  $\ell_{\text{best}}$ ; physical verifier  $f_\phi$ ; maximum diffusion timestep  $T$

**Ensure:** Generated video  $\hat{\mathbf{v}}$

- 1: Sample initial noises  $\mathbf{z}_T^{(i)} \sim \mathcal{N}(\mathbf{0}, \mathbf{I})$  for  $i = 1, \dots, N$
- 2: Initialize active trajectory set  $\mathcal{A} \leftarrow \{1, \dots, N\}$
- 3: **for**  $t = T, T - 1, \dots, 1$  **do**
- 4:   **for**  $i \in \mathcal{A}$  **do**
- 5:      $\mathbf{z}_{t-1}^{(i)}, \mathbf{h}_t^{(i)} \leftarrow \text{DiTStep}(\mathbf{z}_t^{(i)}, t, \mathbf{c})$
- 6:      $\mathbf{f}_t^{(i)} \leftarrow \text{PoolFeat}(\mathbf{h}_t^{(i)}; \ell_{\text{best}})$
- 7:   **end for**
- 8:   **if**  $t \in \mathcal{C}$  **then**
- 9:     **for**  $i \in \mathcal{A}$  **do**
- 10:       $s_t^{(i)} \leftarrow f_\phi(\mathbf{f}_t^{(i)})$
- 11:     **end for**
- 12:     Keep only the top  $\lceil \rho |\mathcal{A}| \rceil$  trajectories ranked by  $s_t^{(i)}$
- 13:   **end if**
- 14: **end for**
- 15: Let  $i^*$  be the remaining trajectory in  $\mathcal{A}$
- 16: **return**  $\hat{\mathbf{v}} \leftarrow \text{VaeDecode}(\mathbf{z}_0^{(i^*)})$

---

trajectory selection. Rather than generating complete videos before evaluating them, we maintain  $N$  parallel denoising trajectories from independent initial noise samples  $\{\mathbf{z}_T^{(i)}\}_{i=1}^N$  and progressively eliminate physically implausible candidates.

**Algorithm.** Let  $\mathcal{C} \subseteq \mathcal{T}$  denote the checkpoint timesteps used for progressive selection, ordered from high to low noise. At each checkpoint, the physical verifier evaluates all active trajectories using their intermediate frame-level features extracted at layer  $\ell_{\text{best}}$ , and only the top fraction  $\rho$  are retained for further denoising. With a fixed keep ratio  $\rho$ , the number of active trajectories decreases geometrically across checkpoints, thereby focusing compute on the most promising candidates. Algorithm 1 and Figure 1 summarize the procedure.

**Design choices.** Two design choices deserve clarification. First, Sec. 3 shows PC separability is more reliable at moderate noise, so we place checkpoints only after entering this regime (avoiding very early, noise-dominated steps). Second, we select using only the physical common-sense score; adding the semantic score did not improve quality in our preliminary experiments, likely because semantic alignment is already promoted by classifier-free guidance.

**Addressing the verifier bottleneck.** A key limitation of post-hoc selection methods is that pixel-space verifiers exhibit poor temporal coherence when applied to noisy intermediate samples [5], making early selection unreliable. Our physical verifier largely avoids this issue. Because it is trained directly on noisy DiT features at the same timesteps where selection occurs, it can provide reliable plausibility estimates even at relatively high noise levels (e.g.,  $t=600$ ). This enables aggressive early pruning, where computational savings are greatest.

**Computational cost.** Let  $T_{\text{steps}}$  denote the total number of DDIM steps. With keep ratio  $\rho$  and  $K$  checkpoints spaced approximately evenly across the schedule, the expected number of DiT forward passes is

$$C_{\text{ours}} \approx T_{\text{steps}} \cdot N \cdot \frac{1 - \rho^{K+1}}{(K+1)(1-\rho)}. \quad (5)$$

For example, with  $N=4$ ,  $K=2$ , and checkpoints at  $t \in \{600, 400\}$ , the active pool shrinks as  $4 \rightarrow 2 \rightarrow 1$ . Under our 50-step DDIM schedule, this corresponds to roughly 20 steps with 4 trajectories, 10 steps with 2, and 20 steps with 1, totaling about 120 DiT forward passes. By comparison, Best-of-4 requires 200 forward passes, corresponding to an  $\approx 1.7\times$  *speedup* in generation. The physical verifier itself adds negligible overhead relative to a DiT forward pass.

## 5 Experiments

### 5.1 Setup

**Training data.** Following the matched-distribution principle established in Sec. 3.2, we train the physics verifier exclusively on CogVideoX-2B-generated videos to match the inference-time distribution. We use 343 videos from VideoPhy [3] generated by CogVideoX-2B, with binary physical plausibility annotations. For each video, we apply forward diffusion at timesteps  $t \in \{200, 400, 600\}$ , yielding  $\sim 1\text{K}$  training samples after an 85%/15% train/validation split (random, seed=42). Despite the modest dataset size, the physics head has a compact architecture ( $\sim 0.8\text{M}$  parameters) and trains reliably with early stopping based on validation AUC. The final model achieves a validation AUC of 0.68, consistent with the probe-level signal strength observed in Sec. 3.

**Physics Verifier.** We use the causal-head architecture described in Sec. 4.1, operating on frozen DiT layer-15 features. Training uses AdamW [25] with learning rate  $10^{-3}$ , weight decay 0.01, batch size

Table 3: **PhyGenBench results** (CogVideoX-2B, 160 prompts, 27 physical laws). S1: VQAScore (single-frame), S2: multi-frame physics (GPT-4o), S3: naturalness (GPT-4o). †Official results from [26] under a different evaluation configuration. Best per-column in **bold** among comparable runs.

Method	Overall	S1	S2	S3	Mech.	Opti.	Ther.	Mate.	Time (s)
CogVideoX-2B†	0.370	–	–	–	0.38	0.43	0.34	0.39	204
Random Sel.	0.490	1.944	0.875	1.563	<b>0.508</b>	0.533	0.444	0.450	477
Best-of-4	<b>0.515</b>	1.963	0.869	<b>1.731</b>	0.500	<b>0.587</b>	0.456	0.483	778
Ours	<b>0.515</b>	<b>1.981</b>	<b>0.913</b>	1.694	0.492	0.580	<b>0.467</b>	<b>0.492</b>	490

32, and OneCycleLR scheduling with 10% warmup. We apply early stopping with patience of 20 epochs on validation AUC. To handle class imbalance ( $\sim 35\%$  physically plausible), we use weighted binary cross-entropy with `pos.weight` =  $n_{\text{neg}}/n_{\text{pos}}$ . Training completes in under 10 minutes on a single GPU.

**Video generation.** We use CogVideoX-2B [42] as the base video diffusion model. Videos are generated with 50 DDIM steps at  $480 \times 720$  resolution and contain 49 frames. We use classifier-free guidance with scale 6.0. For trajectory selection, we initialize  $N = 4$  parallel denoising trajectories and apply progressive pruning at checkpoints  $t \in \{600, 400\}$  with keep ratio  $\rho = 0.5$ , reducing the active pool as  $4 \rightarrow 2 \rightarrow 1$ .

**Evaluation.** We evaluate on PhyGenBench [26], which contains 160 prompts spanning 27 physical laws across four categories: mechanics, optics, thermal, and material properties. We follow the official PhyGenEval protocol: (1) VQAScore [21] using CLIP-FlanT5-XXL for single-frame physical phenomena detection (Stage 1); (2) multi-frame physics verification using GPT-4o [27] for temporal ordering of physical events (Stage 2); and (3) video-level naturalness rating on a 0–3 scale using GPT-4o (Stage 3). Per-video scores are aggregated following the official protocol. In addition, we conduct pairwise comparisons using GPT-4o as judge, presenting two videos side-by-side (order randomized) and asking which better demonstrates the described physical phenomenon.

**Baselines.** We compare against: (1) **Baseline**: standard CogVideoX-2B generation with a single random seed; (2) **Random Selection**: trajectory pruning with random scores instead of physics head scores, isolating the effect of multi-trajectory sampling from physics-informed guidance; (3) **Best-of-4**: generate four complete videos and select the best by physics head score at  $t=200$ ; and (4) reported PhyGenBench results for CogVideoX-2B [26]. We additionally evaluate our approach on other video diffusion backbones in the supplementary.

Table 4: **Pairwise preference** judged by GPT-4o (160 prompts, presentation order randomized).

Comparison	Ours	Tie	Other
Ours vs. Baseline	<b>50.0%</b>	24.4%	25.6%
Ours vs. Random Sel.	<b>31.2%</b>	47.5%	20.6%
Ours vs. Best-of-4	8.1%	86.9%	5.0%

## 5.2 Results

**PhyGenBench evaluation.** Table 3 reports results on PhyGenBench. Our method matches Best-of-4 in overall score (0.515) while achieving the highest Stage 2 score (0.913)—the metric most directly measuring multi-frame physical consistency. Compared to Random Selection, which uses the same pruning mechanism but with uninformed scores, our method improves from 0.490 to 0.515, confirming that physics-guided selection is responsible for the gain. Improvements are consistent across three of four categories, with the largest gains in material properties (+0.042) and thermal phenomena (+0.023).

**Pairwise comparison.** Table 4 reports GPT-4o pairwise judgments. Our method is preferred over single-seed baseline in 50.0% of cases (vs. 25.6% baseline preferred). Part of this gain stems from the multi-trajectory setup itself: even Random Selection outperforms the baseline (55.6% vs. 18.8%). However, comparing our method directly against Random Selection confirms that physics-informed scoring provides additional benefit (31.2% ours preferred vs. 20.6% random preferred, with 47.5% ties). Against Best-of-4, the two methods are largely indistinguishable (86.9% ties), consistent with their matching PhyGenBench scores.

**Efficiency.** The key advantage of progressive selection over Best-of-4 is reduced compute. As shown in the Time column of Table 3, Best-of-4 runs all four trajectories to completion ( $4 \times 50 = 200$  total denoising steps). In contrast, our method terminates two trajectories at  $t=600$  and one more at  $t=400$ , resulting in a **37%** reduction in wall-clock time (490s vs. 778s) while achieving output quality comparable to Best-of-4 (Table 3, Table 4). The additional cost of the physics head forward pass at each checkpoint is small (less than 3% of total generation time), introducing only minimal overhead compared to Random Selection <sup>1</sup>

<sup>1</sup> All experiments run on a single NVIDIA A5000. Wall-clock time includes prompt encoding, denoising, and video decoding.

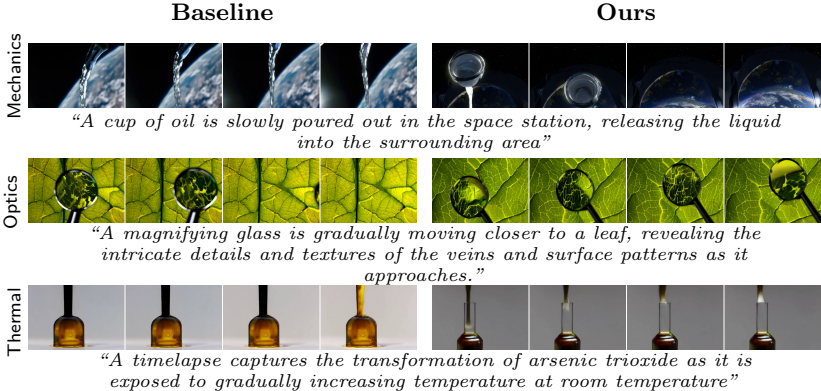


Fig. 4: **Qualitative comparison** on PhyGenBench prompts (4 uniformly sampled frames per video). **Mechanics**: baseline pours oil downward under terrestrial gravity; ours forms a floating liquid mass consistent with microgravity. **Optics**: the texture magnified through the baseline’s lens appears incoherent with the surrounding leaf venation; ours produces a magnified view whose structure is consistent with the underlying leaf surface. **Thermal and Physical Properties**: baseline shows a liquid stream (incorrect); ours shows rising vapor consistent with sublimation.

## 6 Discussion and Conclusion

We have shown that frozen DiT intermediate features carry a measurable signal of physical plausibility that is not reducible to generic perceptual/alignment cues or generator identity. A lightweight physical verifier trained on these features enables progressive trajectory selection that matches Best-of-4 quality while reducing wall-clock generation time by 37%. Taken together, the probing analysis in Section 3 and the downstream results in Section 5 suggest that video diffusion transformers acquire implicit physical knowledge as a byproduct of learning to denoise, even without explicit physics supervision.

Several limitations remain. First, the probing signal is moderate, which limits the achievable selection accuracy when candidate trajectories differ only subtly in physical plausibility. Second, the matched-distribution requirement (Section 3.2) currently necessitates training a verifier per base model, reducing plug-and-play generalization across generators and backbones. Third, our verifier is trained on a limited set of labeled videos and may not generalize to physical phenomena that are underrepresented in the current dataset. Finally, our evaluation fol-

lows PhyGenEval and relies on GPT-4o [27], inheriting the noise and potential bias of VLM-based judging.

These limitations suggest directions for future work. Scaling training data with synthetic or simulator-generated scenarios could strengthen the signal and broaden physical coverage. Extending the analysis to larger DiTs and additional backbones would clarify how such representations scale with model capacity. Finally, combining selection with lightweight test-time steering [24,45,14] may further close the gap to physics-aware fine-tuning while preserving the modularity and efficiency of our approach.

In summary, we show that signals correlated with physical plausibility are recoverable from intermediate representations of video diffusion models, and that even a modest signal can be practically useful for early trajectory pruning. We hope this work encourages further study of what generative models encode about physical plausibility and how such signals can be leveraged at inference time.

## References

1. Akkerman, R., Feng, H., Black, M.J., Tzionas, D., Abrevaya, V.F.: Interdyn: Controllable interactive dynamics with video diffusion models. In: Proceedings of the IEEE/CVF Conference on Computer Vision and Pattern Recognition (CVPR) (2025)
2. Bai, S., et al.: Qwen2.5-VL: Scaling vision-language models for perception, reasoning, and agent (2025)
3. Bansal, H., Lin, Z., Xie, T., Zong, Z., Yarom, M., Bitton, Y., Jiang, C., Sun, Y., Chang, K.W., Grover, A.: VideoPhy: Evaluating physical commonsense for video generation (2024)
4. Bansal, H., Peng, C., Bitton, Y., Goldenberg, R., Grover, A., Chang, K.W.: VideoPhy-2: A challenging action-centric physical commonsense evaluation in video generation (2025)
5. Baraldi, L., Cornia, M., Cucchiara, R.: Verifier matters: Enhancing inference-time scaling for video diffusion models. In: Proceedings of the British Machine Vision Conference (BMVC) (2025)
6. Blattmann, A., Timofte, R., et al.: Stable video diffusion: Scaling latent video diffusion models to large datasets. arXiv preprint arXiv:2311.15127 (2023)
7. Brooks, T., Peebles, B., Holmes, C., DePue, W., Guo, Y., Jing, L., Schnurr, D., Taylor, J., Luhman, T., Luhman, E., Ng, C., Wang, R., Ramesh, A.: Video generation models as world simulators. [urlhttps://openai.com/research/video-generation-models-as-world-simulators](https://openai.com/research/video-generation-models-as-world-simulators) (2024)
8. Cai, Y., Li, K., Jia, M., Wang, J., Sun, J., Liang, F., Chen, W., Juefei-Xu, F., Wang, C., Thabet, A., et al.: PhyGDPO: Physics-aware group-

- wise direct preference optimization for physically consistent text-to-video generation (2025)
9. Caron, M., Touvron, H., Misra, I., Jégou, H., Mairal, J., Bojanowski, P., Joulin, A.: Emerging properties in self-supervised vision transformers. In: ICCV (2021)
  10. Cerspense: zeroscope\_v2: A watermark-free modelscope-based video model. [https://huggingface.co/cerspense/zeroscope\\_v2\\_576w](https://huggingface.co/cerspense/zeroscope_v2_576w) (2023)
  11. Chen, H., Zhang, Y., Cun, X., Xia, M., Wang, X., Weng, C., Shan, Y.: Videocrafter2: Overcoming data limitations for high-quality video diffusion models. In: Proceedings of the IEEE/CVF conference on computer vision and pattern recognition (2024)
  12. Dhariwal, P., Nichol, A.: Diffusion models beat GANs on image synthesis. In: Advances in Neural Information Processing Systems (NeurIPS) (2021)
  13. Geng, D., Herrmann, C., Hur, J., Cole, F., Zhang, S., Pfaff, T., Lopez-Guevara, T., Aytar, Y., Rubinstein, M., Sun, C., Wang, O., Owens, A., Sun, D.: Motion prompting: Controlling video generation with motion trajectories. In: Proceedings of the IEEE/CVF Conference on Computer Vision and Pattern Recognition (CVPR) (2025)
  14. Gillman, N., Herrmann, C., Freeman, M., Aggarwal, D., Luo, E., Sun, D., Sun, C.: Force prompting: Video generation models can learn and generalize physics-based control signals. arXiv preprint arXiv:2505.19386 (2025), <https://arxiv.org/abs/2505.19386>
  15. Gillman, N., et al.: Goal force: Teaching video models to accomplish physics-conditioned goals. arXiv preprint arXiv:2601.05848 (2026), <https://arxiv.org/abs/2601.05848>
  16. He, H., Liang, J., Wang, X., Wan, P., Zhang, D., Gai, K., Pan, L.: Scaling image and video generation via test-time evolutionary search. arXiv preprint arXiv:2505.17618 (2025), <https://arxiv.org/abs/2505.17618>
  17. He, X., Jiang, D., Zhang, G., Ku, M., Soni, A., Siu, S., Chen, H., Chandra, A., Jiang, Z., Arulraj, A., et al.: VideoScore: Building automatic metrics to simulate fine-grained human feedback for video generation (2024)
  18. Kang, B., Yue, Y., Lu, R., Lin, Z., Zhao, Y., Wang, K., Huang, G., Feng, J.: How far is video generation from world model? A physical law perspective. In: International Conference on Machine Learning (ICML) (2025)
  19. Kong, W., Tian, Q., Zhang, Z., Min, R., Dai, Z., Zhou, J., Xiong, J., Xiao, X., et al.: HunyuanVideo: A systematic framework for large video generative models (2024)
  20. Li, C., et al.: Pisa experiments: Exploring physics post-training for video diffusion models by watching stuff drop (2025)
  21. Lin, Z., Pathak, D., Li, B., Li, J., Xia, X., Neubig, G., Zhang, P., Ramanan, D.: Evaluating text-to-visual generation with image-to-text generation. In: European Conference on Computer Vision (2024)

22. Liu, J., Liu, G., Liang, J., Yuan, Z., Liu, X., Zheng, M., Wu, X., Wang, Q., Qin, W., Xia, M., Wang, X., Liu, X., Yang, F., Wan, P., Zhang, D., Gai, K., Yang, Y., Ouyang, W.: Improving video generation with human feedback. In: Advances in Neural Information Processing Systems (2025), arXiv:2501.13918
23. Liu, S., Ren, Z., Gupta, S., Wang, S.: PhysGen: Rigid-body physics-grounded image-to-video generation (2024)
24. Liu, T., Zeng, H., Li, Y., Yi, H., Chang, Y.H., Song, S., Fu, J., Yang, J., Liu, H.Y., Zhu, J., Guibas, L.J.: PhysDreamer: Physics-based interaction with 3D objects via video generation (2024)
25. Loshchilov, I., Hutter, F.: Decoupled weight decay regularization. In: International Conference on Learning Representations (ICLR) (2019)
26. Meng, F., Liao, J., Tan, X., Shao, W., Lu, Q., Zhang, K., Yu, C., Li, D., Qiao, Y., Luo, P.: Towards world simulator: Crafting physical commonsense-based benchmark for video generation. In: International Conference on Machine Learning (ICML) (2025)
27. OpenAI: GPT-4o system card. <https://openai.com/index/gpt-4o-system-card/> (2024)
28. Oshima, Y., Suzuki, M., Matsuo, Y., Furuta, H.: Inference-time text-to-video alignment with diffusion latent beam search. arXiv preprint arXiv:2501.19252 (2025)
29. Polyak, A., Zohar, A., Brown, A., Tjandra, A., Sinha, A., Lee, A., Vyas, A., Shi, B., Ma, C.Y., Chuang, C.Y., et al.: Movie gen: A cast of media foundation models (2024)
30. Prabhudesai, M., Mendonca, R., Luo, Z., Xie, S., Pathak, D., Ehsani, K., Fragkiadaki, K.: Video diffusion alignment via reward gradients (2024)
31. Raghu, M., Unterthiner, T., Kornblith, S., Zhang, C., Dosovitskiy, A.: Do vision transformers see like convolutional neural networks? In: NeurIPS (2021)
32. Rombach, R., Blattmann, A., Lorenz, D., Esser, P., Ommer, B.: High-resolution image synthesis with latent diffusion models. In: Proceedings of the IEEE/CVF conference on computer vision and pattern recognition (2022)
33. Romero, D., Bermudez, A., Li, H., Pizzati, F., Laptev, I.: Learning to generate object interactions with physics-guided video diffusion. arXiv preprint arXiv:2510.02284 (2025), <https://arxiv.org/abs/2510.02284>
34. RunwayML: Runway gen-2: Text to Video Generation. <https://runwayml.com/research/gen-2> (2023), accessed: 2026-03-04
35. Wan Team: Wan: Open and advanced large-scale video generative models (2025)
36. Wang, C., Chen, C., Huang, Y., Dou, Z., Liu, Y., Gu, J., Liu, L.: Physctrl: Generative physics for controllable and physics-grounded video generation. arXiv preprint arXiv:2509.20358 (2025), <https://arxiv.org/abs/2509.20358>
37. Wang, J., Ma, A., Cao, K., Zheng, J., Feng, J., Zhang, Z., Pang, W., Liang, X.: Wisa: World simulator assistant for physics-aware text-to-video generation. In: The Thirty-ninth Annual Conference on Neural Information Processing Systems (2025)

38. Wang, T., Zhou, C., Sun, Q., Zhang, H.: Causal attention for unbiased visual recognition. In: Proceedings of the IEEE/CVF international conference on computer vision (2021)
39. Wang, Y., Chen, X., Ma, X., Zhou, S., Huang, Z., Wang, Y., Yang, C., He, Y., Yu, J., Yang, P., et al.: Lavie: High-quality video generation with cascaded latent diffusion models. *International Journal of Computer Vision* (2025)
40. Wu, X., Huang, S., Wang, G., Xiong, J., Wei, F.: Boosting text-to-video generative model with mllms feedback. In: *Advances in Neural Information Processing Systems* (2024)
41. Yang, X., et al.: VLIPP: Towards physically plausible video generation with vision and language informed physical prior. In: *International Conference on Computer Vision (ICCV)* (2025)
42. Yang, Z., Teng, J., Zheng, W., Ding, M., Huang, S., Xu, J., Yang, Y., Hong, W., Zhang, X., Feng, G., Yin, D., Zhang, Y., Wang, W., Cheng, Y., Bin, X., Gu, X., Dong, Y., Tang, J.: CogVideoX: Text-to-video diffusion models with an expert transformer. In: *International Conference on Learning Representations (ICLR)* (2025)
43. Yu, J., Wang, Y., Zhao, C., Ghanem, B., Zhang, J.: Freedom: Training-free energy-guided conditional diffusion model. In: *Proceedings of the IEEE/CVF International Conference on Computer Vision (ICCV)* (2023)
44. Yuan, H., Zhang, S., Wang, X., Wei, Y., Feng, T., Pan, Y., Zhang, Y., Liu, Z., Albanie, S., Ni, D.: InstructVideo: Instructing video diffusion models with human feedback (2024)
45. Yuan, Y., Wang, X., Wickremasinghe, T., Nadir, Z., Ma, B., Chan, S.H.: Newtongen: Physics-consistent and controllable text-to-video generation via neural newtonian dynamics. *arXiv preprint arXiv:2509.21309* (2025)
46. Zhang, K., Xiao, C., Xu, J., Mei, Y., Patel, V.M.: Think before you diffuse: Llms-guided physics-aware video generation. *arXiv preprint arXiv:2505.21653* (2025)
47. Zhang, X., Liao, J., Zhang, S., Meng, F., Wan, X., Yan, J., Cheng, Y.: Videorepa: Learning physics for video generation through relational alignment with foundation models. In: *Advances in Neural Information Processing Systems* (2025)
48. Zhang, Z., Liao, J., Li, M., Dai, Z., Qiu, B., Zhu, S., Qin, L., Wang, W.: Tora: Trajectory-oriented diffusion transformer for video generation. In: *Proceedings of the IEEE/CVF Conference on Computer Vision and Pattern Recognition (CVPR)* (2025)
49. Zheng, Z., Peng, X., Yang, T., Shen, C., Li, S., Liu, H., Zhou, Y., Li, T., You, Y.: Open-Sora: Democratizing efficient video production for all (2024)

# Appendix

This appendix provides additional implementation details (cf. Section A), experimental results (cf. Section B), and qualitative examples (cf. Section C) and failure cases (cf. Section D) that complement the main text and help readers better understand our method and contributions.

## A Additional Implementation Details

This section provides additional details on the physics verifier architecture, feature extraction pipeline, and video generation setup, complementing Sections 3–5 of the main paper. Beyond the primary experiments on CogVideoX-2B [42] reported in the main paper, we further evaluate our framework on two additional backbones, CogVideoX-5B [42] and Wan 2.1-14B [35], to assess cross-backbone generalization. The physics verifier architecture is shared across all three settings, with only the input projection layer adapted to the hidden dimension of each backbone.

### A.1 Physics Verifier Architecture

The physics verifier takes as input the spatially pooled per-frame DiT features extracted from layer  $\ell$  at denoising timestep  $t$ , denoted by  $\mathbf{f}_t^{(\ell)} \in \mathbb{R}^{F \times D}$ , where  $F = 13$  is the number of latent frames and  $D$  is the hidden dimension of the backbone. Table 5 presents the full layer-by-layer architecture, while Table 6 summarizes the backbone-specific configurations.

Table 5: Architecture of the proposed physics verifier. The input projection layer is adapted to the hidden dimension  $D$  of the corresponding backbone, while all remaining components are shared across backbones.

Component	Operation	Output Shape
Input	Spatially pooled per-frame DiT features	$[B, F, D]$
Input Projection	Linear( $D \rightarrow d$ )	$[B, F, d]$
Positional Embedding	Add learnable positional embeddings $\mathbf{p}_{1:F} \in \mathbb{R}^{F \times d}$	$[B, F, d]$
Layer Normalization	Pre-normalization	$[B, F, d]$
Causal Self-Attention	Multi-head self-attention ( $h = 4$ ) with a causal mask	$[B, F, d]$
Residual Connection	$\hat{\mathbf{f}} + \text{CausalAttn}(\text{LN}(\hat{\mathbf{f}}))$	$[B, F, d]$
Sequence Pooling	Select the final-frame representation	$[B, d]$
Layer Normalization	Apply LayerNorm	$[B, d]$
Classifier Head	Linear( $d \rightarrow 128$ ) $\rightarrow$ GELU $\rightarrow$ Linear( $128 \rightarrow 1$ )	$[B, 1]$
Output	Sigmoid physical plausibility score	$[B, 1]$

Table 6: Backbone-specific configurations of the three DiT backbones evaluated in this work. The physics verifier architecture ( $d = 256$ ,  $h = 4$ ) is shared across all settings; only the input projection layer and the feature extraction hook differ across backbones.

	CogVideoX-2B [42]	CogVideoX-5B [42]	Wan 2.1-14B [35]
Hidden dimension $D$	1920	3072	5120
Number of transformer layers	30	42	40
Text tokens in sequence	Yes (226 tokens)	Yes (226 tokens)	No (cross-attention)
Feature extraction hook	<code>transformer_blocks</code>	<code>transformer_blocks</code>	<code>blocks</code>
Positional encoding	Learned	Rotary (RoPE)	—
Sampling scheduler	DDIM	DDIM	UniPCMultistep
Verifier parameters	$\sim 0.55\text{M}$	$\sim 0.85\text{M}$	$\sim 1.37\text{M}$
Verifier input shape	[13, 1920]	[13, 3072]	[13, 5120]

**Design choices.** The causal self-attention mask ensures that the representation at frame  $i$  attends only to frames  $j \leq i$ , thereby enforcing temporal causality. This design is motivated by the observation that physical violations often emerge as progressively accumulated inconsistencies over time (e.g., an object gradually deviating from a physically plausible trajectory across successive frames). Using the final-frame representation as the sequence summary allows the verifier to aggregate information from all preceding frames while preserving causal ordering. We use  $d = 256$  and  $h = 4$  attention heads in all experiments. The parameter count is dominated by the input projection layer,  $\text{Linear}(D \rightarrow d)$ , and therefore scales with the backbone hidden dimension  $D$ : from approximately 0.55M parameters for CogVideoX-2B [42] ( $D = 1920$ ) to approximately 1.37M for Wan 2.1-14B [35] ( $D = 5120$ ). Even in the largest setting, the verifier introduces less than 0.01% additional parameters relative to the backbone.

**Backbone-specific differences in feature extraction.** The three backbones differ primarily in their text-conditioning mechanisms. CogVideoX-2B [42] and CogVideoX-5B [42] prepend 226 T5 text tokens to the video-token sequence, and we remove these text tokens during feature extraction. By contrast, Wan 2.1-14B [35] uses cross-attention for text conditioning, so its hidden states contain only video tokens. In addition, CogVideoX-5B requires explicit rotary positional embeddings (`image_rotary_emb`) at each transformer forward pass; otherwise, generation collapses to all-black outputs. Finally, because the UniPCMultistep scheduler used by Wan 2.1-14B is stateful, we maintain a separate deep-copied scheduler for each parallel trajectory during multi-trajectory generation.

Table 7: Training hyperparameters of the physics verifier, shared across all backbones.

Hyperparameter	Value
Optimizer	AdamW
Learning rate	$1 \times 10^{-3}$
Weight decay	0.01
Batch size	32
Learning-rate schedule	OneCycleLR (10% warmup followed by cosine annealing)
Early stopping	Patience of 20 epochs based on validation AUC
Loss function	Weighted binary cross-entropy ( $\text{pos.weight} = n_{\text{neg}}/n_{\text{pos}}$ )
Training timesteps	{200, 400, 600} (pooled)
Projection dimension $d$	256
Number of attention heads	4

## A.2 Training Details

**Training data.** Following the matched-distribution principle, we train the physics verifier exclusively on CogVideoX-2B-generated videos from VideoPhy [3] and VideoPhy-2 [4]. Combining all available training and test splits yields approximately 2,000 videos with binary physical-commonsense labels. We then apply a random 85%/15% split (seed = 42) to construct the training and validation sets. For each video, we extract DiT features at three timesteps,  $t \in \{200, 400, 600\}$ , effectively increasing the number of training samples to approximately 6,000. The extracted features are stored as fp16 tensors of shape  $[13, D]$ . For the CogVideoX-5B and Wan 2.1-14B experiments, we use the corresponding frozen backbone to extract features from the same VideoPhy videos originally generated by CogVideoX-2B<sup>2</sup>, and train a backbone-matched verifier on these features. As discussed in Section 3.2 of the main paper, the probing signal degrades across generators, making matched-source feature extraction important for effective verifier training.

**Training hyperparameters.** Table 7 summarizes the training configuration, which is kept identical across all three backbones. To address class imbalance (approximately 35% positive samples), we use weighted binary cross-entropy with  $\text{pos.weight} = n_{\text{neg}}/n_{\text{pos}}$ . Training completes in under 10 minutes on a single GPU for each backbone.

**Layer selection.** We train separate physics verifiers for candidate layers  $\ell \in \{5, 10, 15, 20, 25\}$  and select the best-performing layer based on validation-set performance. For CogVideoX-2B, layer  $\ell = 10$  achieves

<sup>2</sup> An alternative is to generate new videos with each backbone and obtain labels via VLM-based auto-annotation. We leave this direction to future work.

the highest validation AUC (approximately 0.79) with the CAUSAL-SIMPLE verifier, substantially outperforming the linear probing baseline (approximately 0.64) reported in Table 2 of the main paper. This gain likely arises from the verifier’s causal temporal modeling, which captures sequential dependencies beyond what a flat linear probe can represent. For consistency, we use the same layer choice ( $\ell = 10$ ) for the CogVideoX-5B and Wan 2.1-14B experiments.

### A.3 Feature Extraction Pipeline

**DiT feature dimensions.** CogVideoX (both 2B and 5B) processes video latents as a flattened sequence of spatio-temporal tokens. For 49-frame videos at  $480 \times 720$  resolution, the VAE produces latent tensors of shape  $[13, C, 60, 90]$ , corresponding to 13 temporal frames with spatial resolution  $60 \times 90$ . The DiT then patchifies and flattens these latents into  $13 \times 30 \times 45 = 17,550$  video tokens, with 226 text-conditioning tokens prepended to the sequence. At each layer, we extract the full hidden state  $\mathbf{h}^{(\ell)} \in \mathbb{R}^{(226+17,550) \times D}$ , discard the first 226 text tokens, reshape the remaining video tokens into  $[13, 30 \times 45, D]$ , and mean-pool over the spatial dimension to obtain  $\mathbf{f}^{(\ell)} \in \mathbb{R}^{13 \times D}$ . For Wan 2.1-14B, text conditioning is applied exclusively through cross-attention, so the hidden states contain only video tokens. The extraction pipeline is therefore simpler: we reshape the video-token sequence from  $[B, T \cdot H \cdot W, D]$  to  $[B, T, H \cdot W, D]$  and then mean-pool over the spatial dimension. No text-token removal is required.

**Hook mechanism.** Features are extracted via a PyTorch forward hook registered on the target transformer block. For CogVideoX, the hook is attached to `transformer.transformer_blocks[\ell]`, whereas for Wan it is attached to `transformer.blocks[\ell]` due to differences in module naming. The hook records the *output* of the transformer block after the residual connection, rather than intermediate attention or MLP activations. Because these features are already computed during the standard forward pass, the additional computational overhead is negligible.

**Text conditioning.** CogVideoX adopts a hybrid text-conditioning scheme. Specifically, text information is injected via cross-attention in every transformer block, while text tokens are also concatenated with video tokens in the input sequence. During feature extraction, we provide the text prompt and therefore obtain text-conditioned features, but discard the explicit text tokens from the extracted hidden states, retaining only the video-token representations. As a result, textual information is reflected implicitly through the conditioned video features rather than through explicit text-token features. By contrast, Wan 2.1-

14B performs text conditioning exclusively through cross-attention, and text tokens are never concatenated with the video-token sequence. This removes the need for text-token stripping and leads to a simpler feature extraction pipeline.

#### A.4 Video Generation Configuration

**Base model.** We use CogVideoX-2B [42] as the primary backbone in all main experiments. The model generates 49-frame videos at  $480 \times 720$  resolution using 50 DDIM denoising steps with a classifier-free guidance scale of 6.0. For CogVideoX-5B, we use the same generation settings but reduce the number of DDIM steps to 30 for efficiency. Wan 2.1-14B uses 30 UniPCMultistep sampling steps with the same guidance scale.

**Trajectory selection.** For progressive trajectory selection, we initialize  $N = 4$  parallel trajectories using independent random seeds (defined by the base seed, prompt index, and trajectory index), and perform selection at checkpoints  $t \in \{600, 400\}$  with a keep ratio of  $\rho = 0.5$ . As a result, the number of active trajectories decreases from  $4 \rightarrow 2 \rightarrow 1$  across the two selection stages. This configuration is used consistently across all three backbones. Checkpoints are not placed at  $t=800$  because discrimination at high noise levels is unreliable (Section 3.3), nor at  $t=200$  because late selection in the schedule yields minimal computational savings.

**Scoring at checkpoints.** At each checkpoint, we perform one additional forward pass for each active trajectory using only the conditional (positive) prompt embedding, without classifier-free guidance. The physics verifier then scores the resulting intermediate features. This scoring pass adds less than 0.01 s per trajectory at each checkpoint, which is negligible relative to the cost of denoising.

**VAE decoding.** Only the final surviving trajectory is decoded by the VAE. We enable VAE tiling but disable slicing, as we observed that enabling both simultaneously can produce solid-color artifacts in the 3D causal VAEs used by both CogVideoX and Wan.

**CogVideoX-5B specific notes.** CogVideoX-5B requires explicit rotary positional embeddings (`image_rotary_emb`) computed using a 2D grid that matches the spatial latent dimensions. These embeddings must be provided at every transformer forward pass; omitting them leads to all-black outputs. By contrast, CogVideoX-2B uses learned positional embeddings and does not require this additional input. On L40S GPUs (48 GB), CogVideoX-5B uses two-pass classifier-free guidance (batch size 1 per pass) to remain within VRAM limits. On H100/H200

Table 8: Summary of the video generation configuration for the three backbones evaluated in this work.

Parameter	CogVideoX-2B	CogVideoX-5B	Wan 2.1-14B
Resolution	480 × 720	480 × 720	480 × 720
Number of frames	49 (13 latent frames)	49 (13 latent frames)	49 (13 latent frames)
Sampling steps	50 (DDIM)	30 (DDIM)	30 (UniPCMultistep)
Guidance scale	6.0	6.0	6.0
Classifier-free guidance	Two-pass (24 GB)	Two-pass (L40S) / Single (H100+)	Single-pass
Number of trajectories ( $N$ )	4	4	4
Selection checkpoints ( $C$ )	{600, 400}	{600, 400}	{600, 400}
Keep ratio ( $\rho$ )	0.5	0.5	0.5
Verifier layer	10	10	10
Primary hardware	A5000 (24 GB)	L40S (48 GB)	H200 (80 GB)

Table 9: Wall-clock time breakdown per video across backbones and modes.

Backbone (GPU, steps)	Component	Baseline	Rand. Sel.	Best-of-4	Ours
CogVideoX-2B (A5000 24 GB, 50 steps)	Sampling	183s	454s	732s	448s
	Scoring	—	—	3s	3s
	Decode + offload	60s	60s	60s	60s
	<b>Total</b>	<b>204s</b>	<b>477s</b>	<b>778s</b>	<b>490s</b>
CogVideoX-5B (L40S 48 GB, 30 steps)	Sampling	137s	—	—	357s
	Decode + offload	12s	—	—	12s
	<b>Total</b>	<b>149s</b>	—	—	<b>374s</b>
Wan 2.1-14B (H200 80 GB, 30 steps)	Sampling	117s <sup>†</sup>	—	—	391s
	Decode	1s	—	—	1s
	<b>Total</b>	<b>118s<sup>†</sup></b>	—	—	<b>393s</b>

<sup>†</sup>Estimated on H200. Measured baseline on 2×L40S is ~305s due to cross-GPU overhead.

GPUs (80 GB), we use single-pass classifier-free guidance (batch size 2) for faster generation.

**Wan 2.1-14B specific notes.** Wan 2.1-14B (approximately 28 GB in bf16) fits on a single 80 GB GPU (H200). We observe that distributing Wan across multiple devices can introduce tiling and blurring artifacts.

**Reproducibility.** For prompt  $i$ , the first trajectory is initialized with seed  $42 + i$ , and subsequent trajectories use seeds  $42 + i + 1$ ,  $42 + i + 2$ , and so on. This setup ensures that trajectory 0 in our method shares the same initial noise as the single-seed baseline, enabling a controlled comparison of the effect of trajectory selection.

**Hardware and timing.** Table 9 provides wall-clock time breakdowns per video across all three backbones, measured from SLURM job logs. For CogVideoX-5B, the per-step cost is ~4.6s per trajectory on L40S with single-pass CFG. Under the 4→2→1 schedule across 30 steps,

sampling breaks down as: 12 steps  $\times$  4 trajectories ( $\sim 220$ s), 6 steps  $\times$  2 ( $\sim 55$ s), 12 steps  $\times$  1 ( $\sim 55$ s), plus 6 scoring forwards ( $\sim 27$ s). For Wan 2.1-14B on H200, the per-step cost is  $\sim 3.9$ s per trajectory despite  $5.6\times$  more parameters than CogVideoX-2B, because batch-1 inference is memory-bandwidth bound and H200 provides  $\sim 5.5\times$  higher bandwidth (4,800 GB/s HBM3e vs. 864 GB/s on L40S). The selection checkpoints at steps 20 and 25 reduce per-step cost from  $\sim 15.5$ s (4 trajectories) to  $\sim 8$ s (2) to  $\sim 5.5$ s (1).

## B Additional Experiments

### B.1 Cross-Backbone Generalization

To evaluate whether our framework generalizes beyond the primary CogVideoX-2B backbone, we apply the same progressive trajectory selection pipeline to two additional video diffusion models: CogVideoX-5B ( $D = 3072$ , 42 layers) and Wan 2.1-14B ( $D = 5120$ , 40 layers). For each backbone, we train a matched physics verifier following the protocol described in Section A.2 and evaluate it on the full PhyGenBench [26] benchmark. Implementation details for each backbone are provided in Section A.1.

**CogVideoX-5B.** Table 10 summarizes the results on CogVideoX-5B. The guided method yields a modest overall improvement of  $+0.003$  over the 5B baseline, with the largest gain observed in material properties ( $+0.100$ ), partially offset by decreases in optics ( $-0.037$ ) and thermal effects ( $-0.066$ ). However, the GPT-4o pairwise evaluation suggests a stronger qualitative benefit: our method is preferred in 42.5% of 153 valid comparisons, compared with 28.1% for the baseline, with 29.4% ties. Excluding ties, the guided method wins 60.2% of decided comparisons, indicating perceptual improvements that are not fully reflected by the aggregate PhyGenEval score.

**Wan 2.1-14B.** The guided method achieves a larger improvement on Wan 2.1-14B, with a  $+0.043$  gain in the overall score ( $+7.6\%$ ) and consistent improvements across all four categories (Table 10). The most pronounced gain appears in multi-frame physics consistency (S2:  $+0.19$ ), which is the metric most directly targeted by trajectory selection. Compared with CogVideoX-5B, the stronger result on Wan likely reflects two factors: (i) Wan is a stronger base model (baseline 0.569 vs. 0.363), so its candidate trajectories span a wider quality range, giving the verifier more room to discriminate; and (ii) Wan’s higher-dimensional feature space ( $D = 5120$ ) may encode richer physics-relevant structure. Under the PhyGenBench protocol, the guided Wan

Table 10: Cross-backbone results on PhyGenBench. All methods are evaluated under the closed-source-only PhyGenEval protocol. Rows marked with  $\Delta$  report the improvement of the guided method over the corresponding backbone baseline. CogVideoX-2B results (from Table 3 of the main paper) are included for reference.

Backbone	Method	Final	S1	S2	S3	Mech.	Opti.	Ther.	Mate.	Pairwise Win Rate
CogVideoX-2B	Baseline	0.370*	—	—	—	0.38	0.43	0.34	0.39	—
	Guided (Ours)	<b>0.515</b>	1.98	<b>0.91</b>	1.69	0.49	0.58	0.47	0.49	<b>66.1%</b>
CogVideoX-5B	Baseline	0.363	1.54	<b>0.58</b>	1.21	0.283	<b>0.493</b>	<b>0.322</b>	0.308	—
	Guided (Ours)	<b>0.365</b>	1.52	0.53	<b>1.30</b>	<b>0.292</b>	0.456	0.256	<b>0.408</b>	<b>62.5%</b>
	$\Delta$	<b>+0.003</b>	-0.02	-0.05	<b>+0.09</b>	<b>+0.009</b>	-0.037	-0.066	<b>+0.100</b>	—
Wan 2.1-14B	Baseline	0.569	2.05	1.28	1.79	0.525	0.740	0.489	0.458	—
	Guided (Ours)	<b>0.612</b>	<b>2.09</b>	<b>1.46</b>	<b>1.86</b>	<b>0.600</b>	<b>0.767</b>	<b>0.533</b>	<b>0.492</b>	—
	$\Delta$	<b>+0.043</b>	<b>+0.04</b>	<b>+0.19</b>	<b>+0.07</b>	<b>+0.075</b>	<b>+0.027</b>	<b>+0.044</b>	<b>+0.033</b>	—

\* Single-seed baseline. For CogVideoX-2B, the pairwise win rate is reported as "Ours vs. Baseline" from Table 4 of the main paper.

result (0.612) compares favorably with the CogVideoX-2B result reported in the PhyGenBench paper [26] (0.37), as well as with several reported closed-source models such as Kling (0.49) and Gen-3 (0.51).

**Summary.** The framework generalizes across architectures with different hidden dimensions, text conditioning schemes, and schedulers. Verifier effectiveness scales with (i) the matched-distribution gap (strongest for 2B where training and inference match) and (ii) base model capability, as stronger baseline provides more discriminable trajectories. Training backbone-matched verifiers on auto-labeled data from each generator is a natural direction for closing the remaining gap.

## B.2 Score Distribution Analysis

Figure 5 compares the verifier’s scoring behavior on CogVideoX-5B and Wan 2.1-14B. On 5B, kept and dropped trajectories show visible separation ( $\Delta_{\text{mean}}=0.071$ ) and per-prompt score spread averages 0.125, indicating the head provides a meaningful selection signal. On Wan, the two distributions nearly completely overlap ( $\Delta_{\text{mean}}=0.019$ ) and score spread averages only 0.034— $3.7\times$  smaller—confirming that the Wan verifier operates near chance and the PhyGenBench improvement (+0.043) is attributable to multi-trajectory diversity rather than physics-informed guidance.

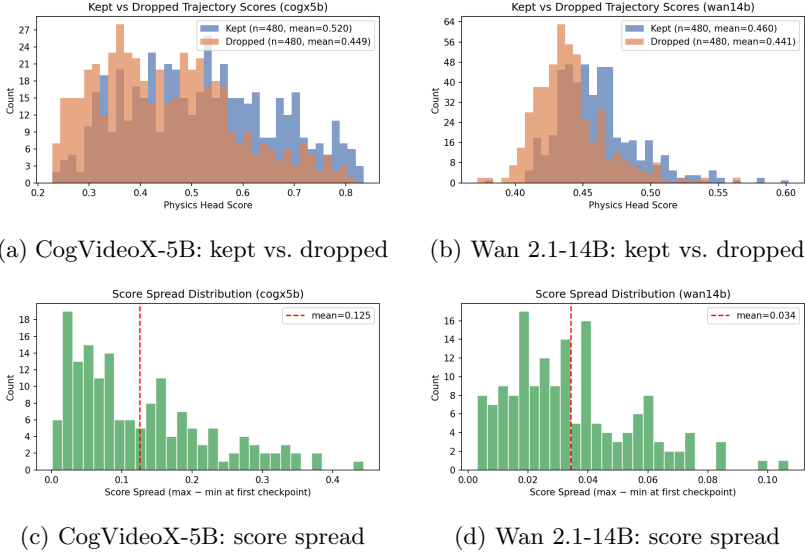


Fig. 5: Verifier score analysis. Top: kept vs. dropped trajectory scores at checkpoints. Bottom: per-prompt score spread (max – min) at the first checkpoint. 5B shows meaningful separation; Wan shows near-complete overlap.

*Per-category analysis.* Figure 6 breaks down verifier scores by the 27 physical law categories in PhyGenBench. On CogVideoX-5B, the verifier exhibits meaningful category-level specialization. It achieves the highest confidence on phenomena characterized by salient temporal state changes—Color mixing (0.693), Deposition (0.675), Boiling (0.668), Tyndall Effect (0.635), and Reflection (0.649)—indicating that the verifier has learned to detect progressive physical dynamics such as phase transitions, light scattering, and color blending from intermediate DiT features. Categories with lower scores, such as Direct Radiation (0.320) and Flame Reaction (0.430), typically involve precise spatial reasoning or domain-specific material knowledge (e.g., shadow geometry, characteristic flame colors), which are underrepresented in the VideoPhy training distribution and suggest a clear avenue for improvement through targeted data augmentation. Notably, this category-dependent structure itself is an informative signal: it demonstrates that the verifier captures physically meaningful distinctions rather than relying on superficial quality cues. On Wan 2.1-14B, category-level variation is substantially reduced—all 29 means fall within  $[0.42, 0.52]$ —

consistent with the distribution mismatch discussed above, and motivating backbone-matched training data as the primary path toward stronger cross-backbone transfer.

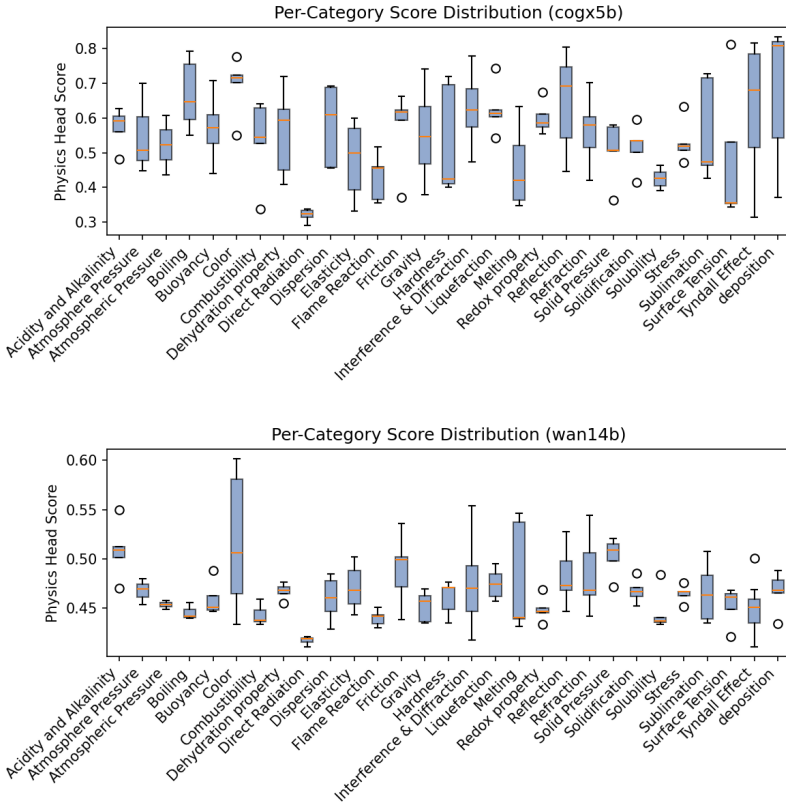


Fig. 6: Per-category score distributions for CogVideoX-5B (top) and Wan 2.1-14B (bottom). On 5B, temporal phenomena (Color, Deposition, Boiling) score highest while spatial/material-specific phenomena (Direct Radiation, Flame Reaction) score lowest. On Wan, categories cluster in  $[0.42, 0.52]$ .

## C More Qualitative Results

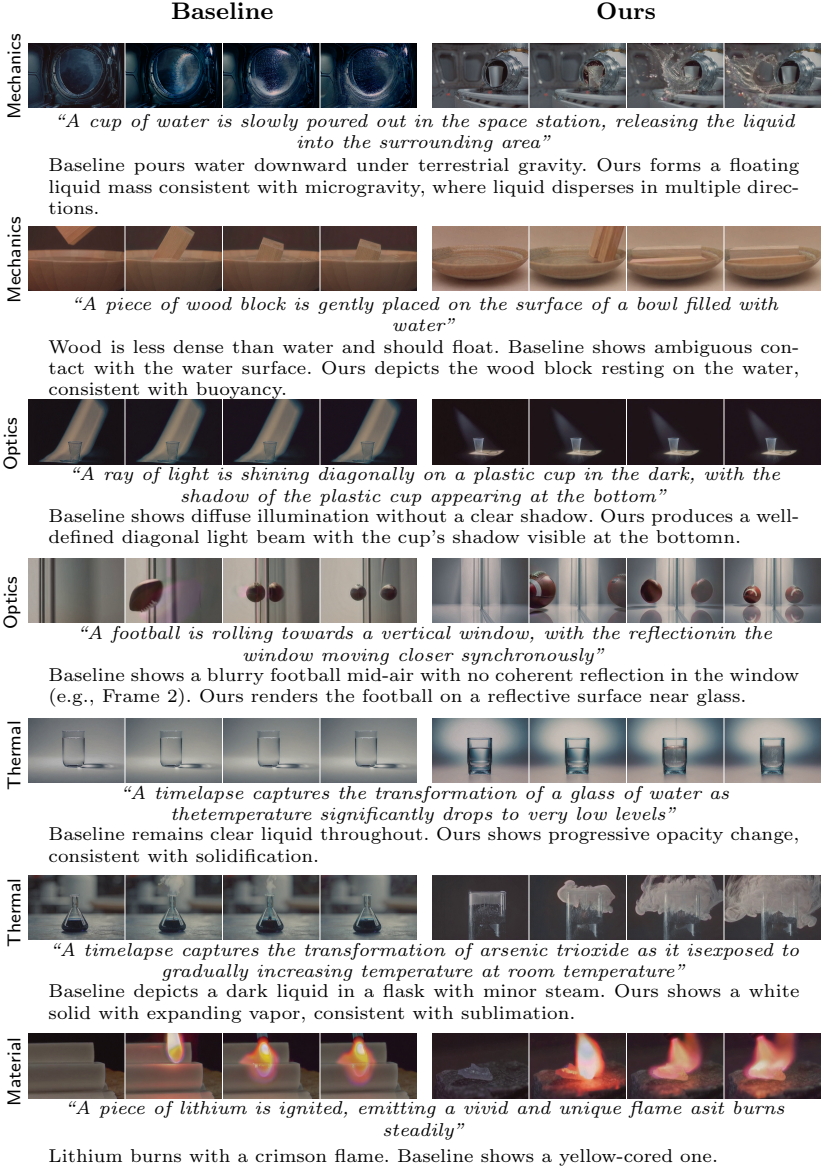
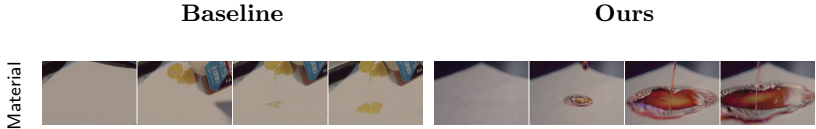


Fig. 7: **Qualitative comparison** on PhyGenBench prompts (Wan-14B, 4 uniformly sampled frames per video). Each row shows baseline (left) vs. guided (right), the generation prompt, and a brief physical analysis.

## D Failure Cases

Figure 8 illustrates representative failure cases. These concentrate in material properties and chemical reaction prompts, which require domain-specific knowledge—such as characteristic flame colors, acid appearances, and fracture mechanics—that goes beyond the common-sense physical reasoning captured by our training data. Moreover, these phenomena inherently involve dramatic transformations in material form (carbonization, shattering, phase changes), which current video diffusion models struggle to synthesize faithfully. When the base model cannot produce any physically correct trajectory, trajectory selection reaches a fundamental ceiling regardless of verifier quality.



*“A timelapse captures the reaction as concentrated sulfuric acid is poured onto a sheet of paper”*

Sulfuric acid is colorless and causes black carbonization. Baseline shows a yellow liquid with no reaction; ours shows a red liquid with paper degradation. Neither depicts the correct acid color or carbonization.



*“A flimsy, brittle glass cup is propelled with force towards a solid, metallic surface, where it collides upon impact”*

The cup should shatter into fragments. Both produce nearly identical results—the cup cracks but never exhibits realistic brittle fracture.

Fig. 8: **Failure cases** (Wan-14B). Both rows show cases where all candidate trajectories are physically incorrect, leaving the verifier unable to select a better outcome.